scientific reports

Check for updates

OPEN

Altered expression and potential role of N6-methyladenosine mRNA methylation in abdominal aortic aneurysm mouse model

Julin Wang[1,4], Tianyu Miao[1,4], Yanyun Wang[2,4], Tiehao Wang[1], Zhangyu He[3], Fei Xiong[1], Ding Yuan[1], Qiang Guo[1], Yi Yang[1], Zhichen Tang[2], Bin Huang[1]✉ & Jichun Zhao[1]✉

It is an important cause of death in old age to rupture an abdominal aortic aneurysm. The pathogenesis of AAA has not been fully elucidated, and m^{6}A RNA methylation regulators have never been implicated in AAA development. This study aimed to explore the expression profile, potential functions and regulated mechanism of m^{6}A RNA methylation in the abdominal aortic aneurysm mice model. A successful AAA mouse model was established using *Ang II*. M^{6}A- methylated RNA Immunoprecipitation (MeRIP) sequencing and RNA sequencing were performed to identify the m^{6}A sites in the abdominal aorta walls samples. The expression of m^{6}A methylation regulators was analyzed in the datasets and MeRIP-qPCR was performed to verify the results of MeRIP-sequencing. Bioinformatics analysis was used to evaluate the m^{6}A patterns and indicate the potential signaling pathway. There were 2039 differentially methylated m^{6}A peaks involving 1865 mRNAs in the AAA group relative to the control, of which 1610 peaks in 1466 mRNAs were hypermethylated, and 429 peaks in 410 mRNAs were hypomethylated. The hypermethylated mRNAs in AAA group were primarily enriched in transcription regulation and intercellular signaling, especially the Wnt signaling-associated processes. Hypomethylated m^{6}A sites were mainly enriched in G protein-coupled receptor activity and ion channel activity. MeRIP-qPCR suggested that the sequencing data were reliable and accurate. The mRNA expression of 24 m^{6}A regulators showed no obvious difference between AAA and the control group, but the m6A methylation levels of three components of methyltransferases complex and one 'readers' were significantly increased. Our study suggested an original viewpoint that the m^{6}A modification might be regulated by several unidentified regulation modes or genes in the *Ang II*-induced AAA mice model, and be closely relevant to the combined effect of m^{6}A methylation modification in the Wnt pathway, G protein-coupled receptor, and ion channel-associated genes, which were worthy of further investigation.

Keywords Abdominal aortic aneurysm, m^{6}A, Methylation, Mice model, Wnt pathway, mRNA

Abdominal aortic aneurysm (AAA) is a dangerous and age-related lethal disease that affects about 8% of older men and 1.3% of older women, which comes with a terribly high mortality of > 50% once ruptured[1]. Ethnicity, age, sex, lifestyle, family history, and cardiovascular diseases are potential contributing factors to AAA[2,3]. Current findings showed that microRNA, single nucleotide polymorphisms, matrix metalloproteinase 9, interleukin -6 receptor, and low-density lipoprotein (LDL) receptor had been differentially expressed in the wall of abdominal aortic aneurysms and normal aorta in human. To dissect the molecular mechanisms underlying AAA, animal models of AAA have been established and widely used, such as angiotensin II (Ang II)-induced apoE$^{-/-}$ mouse model.

[1]Department of Vascular Surgery, West China Hospital, Sichuan University, 37 GuoXue Alley, Chengdu 610041, Sichuan, People's Republic of China. [2]Laboratory of Molecular Translational Medicine, Center for Translational Medicine, Key Laboratory of Birth Defects and Related Diseases of Women and Children, Ministry of Education, West China Second University Hospital, Sichuan University, Chengdu 610041, Sichuan, People's Republic of China. [3]West China School of Basic Sciences and Forensic Medicine, Sichuan University, Chengdu 610041, Sichuan, People's Republic of China. [4]Julin Wang, Tianyu Miao and Yanyun Wang contributed equally to this work. ✉email: dochuangbin@163.com; zhaojc3@163.com

Post-transcriptional modifications in tRNA, rRNA, mRNA, snRNA, snoRNA, miRNA, and viral RNA are involved in multiple biological functions[4]. More than 100 different RNA modifications have been identified so far, two-thirds of which are related to methylation[5]. RNA methylation includes that of adenosine and cytosine, along with isomerization of uridine and ribose[6]. N^6-methyladenosine (m^6A) is mRNA's most abundant methylated residue[7]. m^6A modification is a reversible process in which methyltransferase-like 3(METTL3), methyltransferase-like 14 (METTL14), Wilms' tumor 1-associating protein (WTAP) and KIAA1429 complex acts as m6A "writers", fat mass and obesity-associated Protein (FTO) and AlkB homolog 5 (ALKBH5) as "erasers", and YT521-B homology (YTH) containing proteins and heterogeneous nuclear ribonucleoproteins (HNRNPs) family as "readers". Several findings have proved that m^6A is associated with the immune microenvironment[8,9], downregulation of matrix metallopeptidase[10], oxidative stress[11] etc., which had a close relationship with the mechanisms of AAA. He et al. had reported higher m^6A levels and protein expression of METTL14, FTO, YTHDF1, and YTHDF3 in the AAA tissues compared to the normal aorta in humans[12]. Zhong et al. found that overexpression of METTL3 can promote AAA formation in both Ang II and calcium chloride-induced AAA mouse models[13].

Though these studies have demonstrated that the m^6A modification is likely essential in the development of AAA, none of them focused on the transcriptome-wide m^6A expression. This study aimed to profile the m^6A methylation expression, explore the differential m^6A methylation expression in the aorta walls of the *Ang II*-induced AAA mouse model and normal mice, and further evaluate the function of differential m^6A methylated modification to investigate the underlying mechanisms of AAA in mouse model.

Materials and methods

Ethical approval

Guidelines and regulations were followed in all aspects of the study. All animal experiments were approved by The Animal Care and Use Ethics Committee of West China Second University Hospital, Sichuan University (No.2018084) and in accordance with the ARRIVE (Animal Research: Reporting of In Vivo Experiments, https://arriveguidelines.org) guidelines.

Establishment of AAA model and tissue collection

Male C57BL/6J *apoE*$^{-/-}$ mice (10 to 12 weeks old) were obtained from Gempharmatech. Co., Ltd. (Nanjing, China) and housed under standard conditions. The number of animals enrolled in this study was determined by the requirement of subsequent m^6A sequencing. The AAA model was established according to the protocol of Daugherty et al.[14]. Mice were anesthetized with inhalational isoflurane by Animal Anesthesia System (RWD Life Science, China). The anesthetic induction was performed in an anesthetic induction chamber with 4.0% isoflurane and 100% O_2. The mice were then transferred to the operating floor with maintainable anesthesia of 2.0% isoflurane and 0.6 L/min O_2. Osmotic minipump (Model 2004, Alzet, USA) was filled with Angiotensin II (Ang II, A9525-25, Sigma Chemical Co., USA) which was dissolved with saline. A 1 cm incision which was perpendicular to the spine was made above the acromion on the right side of posterior ear of the mouse. The vessel clamp was inserted into the interior of incision to make a pouch by blunt dissection, and then the minipump was implanted. After the suture of incision, 0.25% bupivacaine was smeared on incision. The anesthesia was ceased, and mice were placed in a recovery room covered by a thermal insulation blanket. The mice were infused with Ang II at a dosage of 1.44 mg/kg·per day through subcutaneously implanted osmotic minipumps. The control group mice were infused with an equal volume of saline for the same duration. The mice were kept in specific pathogen-free (SPF) conditions with regular food and water. Then the mice were euthanized with overdose (100mg/kg) of pentobarbital anesthetization after 28 days, and perfused with saline through the left ventricle of the heart. The whole aorta was harvested from each mouse and snap- frozen in liquid nitrogen for RNA extraction. Or, to prepare the cross section, the sample is fixed for 24 h in 4% paraformaldehyde, cut at the point of maximum diameter, and embedded in paraffin.

RNA treatment

Total RNA was extracted from tissues using RNeasy Micro Kit (74004, Qiagen, Germany), and its ratio for A260/A280 and A260/A230 were measured by NanoDrop (ND-1000), ThermoFisher Scientific, USA). Electrophoresis of denaturing agarose gels was used to test RNA integrity and contaminating gDNA. Ribosomal RNAs (rRNAs) were removed using the NEBNext rRNA Depletion Kit (E6310S, New England Biolabs, USA) according to the manufacturer's instructions. Methylated RNA immunoprecipitation (MeRIP) was performed using the GenSeq™ m^6A-MeRIP Kit (GeneSeq, China), and assessed by Qubit™ Flex Fluorometer (Qubit3, ThermoFisher Scientific, USA). A portion of the isolated RNA was used for library construction.

RNA m^6A sequencing and RNA sequencing

The immunoprecipitated m^6A and total RNA samples from 3 AAA mice and 3 control mice were used for construction of library for RNA-sequencing using NEBNext® Ultra II Directional RNA Library Prep Kit (E7760S, New England Biolabs, USA). The quality of the constructed library was detected with the BioAnalyzer 2100 system (Agilent Technologies, USA). The library was sequenced on the Illumina (NovaSeq 6000, Illumina, USA) platform with 150 bp paired-end reads.

Data analysis

Raw data were collected on the basis of image and base recognition, and reads with Q30 > 80% were analyzed further. Following 3' adaptor trimming and removal of low-quality reads with CUTADAPT software v1.9.3[15], a high-quality read alignment was performed by using Hisat2 software version 2.0.4 with GRCm38/mm10 as the sequence reference (GRCm38/mm10)[16]. Based on fragments per kilobase of exon per million fragments

mapped (FPKM), the expression profiles of high-quality reads were calculated using Ensembl gene annotation file and Cuffdiff software.

m^{6}A methylation regions (peak) on RNAs of each sample were detected by MACS software[17]. The overlaps of m^{6}A methylation regions in intraclass three samples were calculated using Venn Diagrams software, and as the m^{6}A methylation regions of this group. Then the Venn plots, which showed the overlaps of m^{6}A methylation peaks and m^{6}A methylation mRNAs between both groups, were drawn. The sequences of the top 1000 enriched m^{6}A methylation peaks were used to screen the motif by DREME software, and the E-value threshold was set to 0.05[18]. The distribution of characteristic m^{6}A peaks in all transcripts and mRNA regions were generated according to the method of Olarerin-George, et al.[19] and Luo, GZ, et al., respectively[20]. Differentially methylated regions (fold change ≥ 2 and *P*-value ≤ 0.0001) were identified by diffReps software[21]. The common sites identified by both MACS and diffReps software overlapping with mRNA exons were screened. Gene Ontology (GO) analysis in terms of biological process (BP), molecular function (MF) and cellular component annotations, and Kyoto Encyclopedia of Genes and Genomes (KEGG, www.kegg.jp/kegg/kegg1.html) pathway analysis of the differentially methylated mRNAs were performed through the Metascape web tool (https://metascape.org)[22–25].

MeRIP-qPCR

To validate the results of MeRIP-sequencing, two key genes (LEF1 and AXIN1) in Wnt signaling pathway were screened using String online database (https://string-db.org/). The methylated region of LEF1 and AXIN1 mRNA were in 131,223,075–131,223,320 bp on Chr3, and 26,142,861–26,143,576 bp on Chr17, respectively according to the result of MeRIP-sequencing. The potential m^{6}A sites in the two regions were predicted by SRAMP online tool (http://www.cuilab.cn/sramp/) and were evaluated by MeRIP-qPCR method. The specific primers for each m^{6}A site were designed using Primer3 online software (https://primer3.ut.ee/). As the two sites (Chr17: 26,143,008 and Chr17: 26,143,045 in AXIN1 mRNA) were too close to be detected separately by qPCR, a pair of primers was used to detect both of them. The primer used for LEF1 mRNA was as follows: F, CTCCTTCCCAACGTGCAAAG; and R, AGGTTGCTGTCAGTGTTCCT. The primers used for AXIN1 mRNA were as follows: F, TGAGTCACTGCATTCCTTACTG; R, TCATTTGAGTCACAGGGCTC (for Chr17: 26,143,008 and Chr17: 26,143,045); F, GCCATCTACCGAAAGTACATCC; R, CATGGTGGACTGGATTTCTGT (for Chr17:26,143,207); F, GGAGTACACAAGGACAGGCT; R, CCTCATTCAAAGTGGGCAGG (for Chr17: 26,143,335). cDNA for both the immunoprecipitated m^{6}A (IP) and total RNA (Input) samples from 5 AAA mice and 5 control mice were synthesized using Hifair III 1st Strand cDNA Synthesis SuperMix for qPCR (gDNA digester plus) (11141ES60, Yeasen Biotechnology, China). qPCR was performed to evaluate the level of m^{6}A modification of LEF1 and AXIN1 in each sample using SsoFast EvaGreen Supermix (1725200, Bio-Rad Laboratories, USA). The level of methylation was indicated by the IP/input ratio: $\%\text{Input} = 2^{(\text{Ct Input-Ct IP})} \times 1/5 \times 100\%$

Statistical analysis

In order to ensure that quantitative data are normal and homogeneous of variance, the *Shapiro–Wilk* and *Levene's* tests were conducted. The data were then transformed by natural logarithm (Ln) and represented as mean ± SEM. Two independent groups were compared using the *Student's t*-test. A statistically significant difference was considered as $P < 0.05$.

Results

AAA was successfully induced in the Ang II-apoE$^{-/-}$ mice

Relative to saline-infused mice, in *Ang II* saline-infused *apoE*$^{-/-}$ mice, there was a dramatic increase in aortic size of both the lumen and wall (Fig. 1A). Histological analysis of the aortas also showed more severe histopathological destruction, hyperplasia and lumen dilation in the Ang II-pump treated *apoE*$^{-/-}$ mice (Fig. 1B). These data suggested that Ang II-induced AAA mouse model were established successfully.

AAA significantly increased the proportion of m^{6}A-modified mRNAs

M^{6}A-MeRIP sequencing revealed 11,489, 12,386 and 11,821 m^{6}A peaks in 6753, 7035 and 6753 mRNAs in the three AAA samples, as opposed to only 4842, 4208 and 4128 m^{6}A peaks involved in 3262, 2826 and 2864 mRNAs in three control samples. In addition, there were significantly more overlapping m6A peaks (6820 *vs.* 2059) and overlapping methylated mRNAs (5652 vs. 1914) in the AAA samples compared to the control group (Fig. 2A). The distribution of m^{6}A sites across the 5' untranslated region (UTR), start codon region, coding DNA sequence (CDS), stop codon region and 3'UTR were also analyzed. The prevalence of m6A was 12% higher in the CDS regions compared to that in the stop codon regions of the control group, whereas only 2.3% higher rate of m6A was observed in the CDS relative to stop codon regions in the AAA group (Fig. 2B). Furthermore, MetaPlotR analysis of m^{6}A peak density revealed a highest density of m^{6}A peak at the junction between CDS region and 3'UTR in both groups (Fig. 2C). Motif analysis further showed that GGACU was the top enriched methylated site in the AAA group, while GGACKU (K-uracil or guanine) was the top enriched motif in the controls, of which GGACUU had a markedly low E-value. The other methylated motifs in both groups are shown in Fig. 3. Taken together, m^{6}A modification of mRNA is likely involved in the pathogenesis of AAA.

AAA is associated with differential methylation of mRNAs

We identified 2039 differentially methylated m^{6}A peaks in 1865 mRNAs between the AAA and control groups, of which 1610 peaks in 1466 mRNAs were hypermethylated and 429 peaks in 410 mRNAs were hypomethylated. In addition, 91.33% of the hypermethylated mRNAs in AAA group contained only a single hypermethylated m^{6}A peak; among mRNAs with 2–6 hypermethylated peaks, 90.55% had two and 7.87% had three peaks. Interestingly, six hypermethylated m^{6}A peaks were detected in the *TTN* transcript. Most hypomethylated mRNAs in the AAA group had single m^{6}A peaks, and only 3.9% had two or three hypomethylated m^{6}A sites.

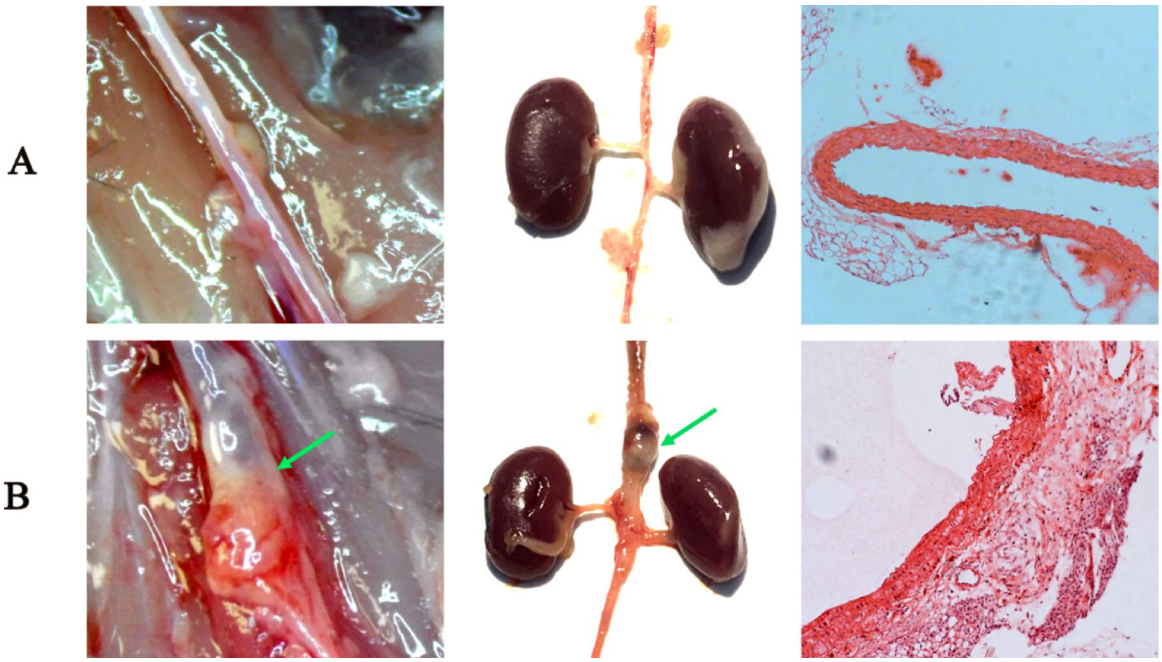

Fig. 1. AAA formation in the angiotensin II treated C57BL/6 J *apoE*$^{-/-}$ mice and histological analysis of the aortas. (**A**) Representative photographs of abdominal aortic fragments and images of Hematoxylin–eosin staining of aortic tissues (10×) in control group. (**B**) Representative photographs of abdominal aortic fragments and images of Hematoxylin–eosin staining of aortic tissues (10×) in AAA group. Green arrows indicated the location of aneurysms.

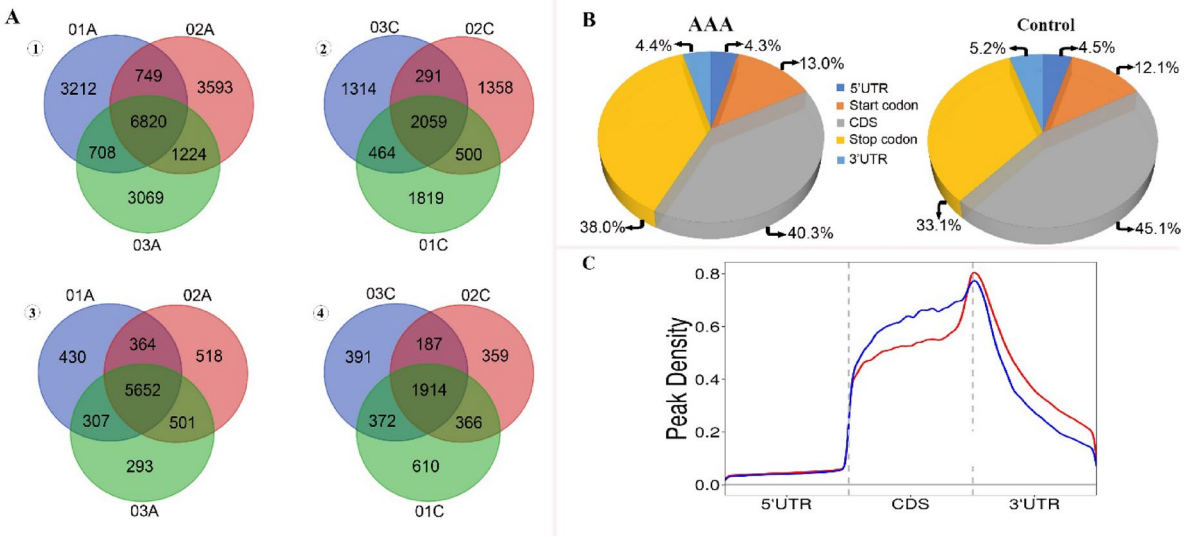

Fig. 2. Overview of m^{6}A methylation modification in AAA and control group. (**A**) Overlapping m^{6}A peaks and methylated mRNAs in the three biological replicates of AAA and control groups; (1) Overlapping m^{6}A peaks in AAA group. (2) Overlapping m^{6}A peaks in control group. (3) Overlapping methylated mRNAs in AAA group. (4) Overlapping methylated mRNAs in control group. 01A, 02A and 03A: AAA group sample 01, 02 and 03; 01C, 02C and 03C: control group sample 01, 02 and 03. (**B**) Pie plot showed the distribution of m^{6}A sites in the five transcript regions in AAA and control groups. (C) Metagen plot showed the average density of m^{6}A peaks in the transcript regions in AAA and control groups. Red curve represents AAA group. Blue curve represents control group.

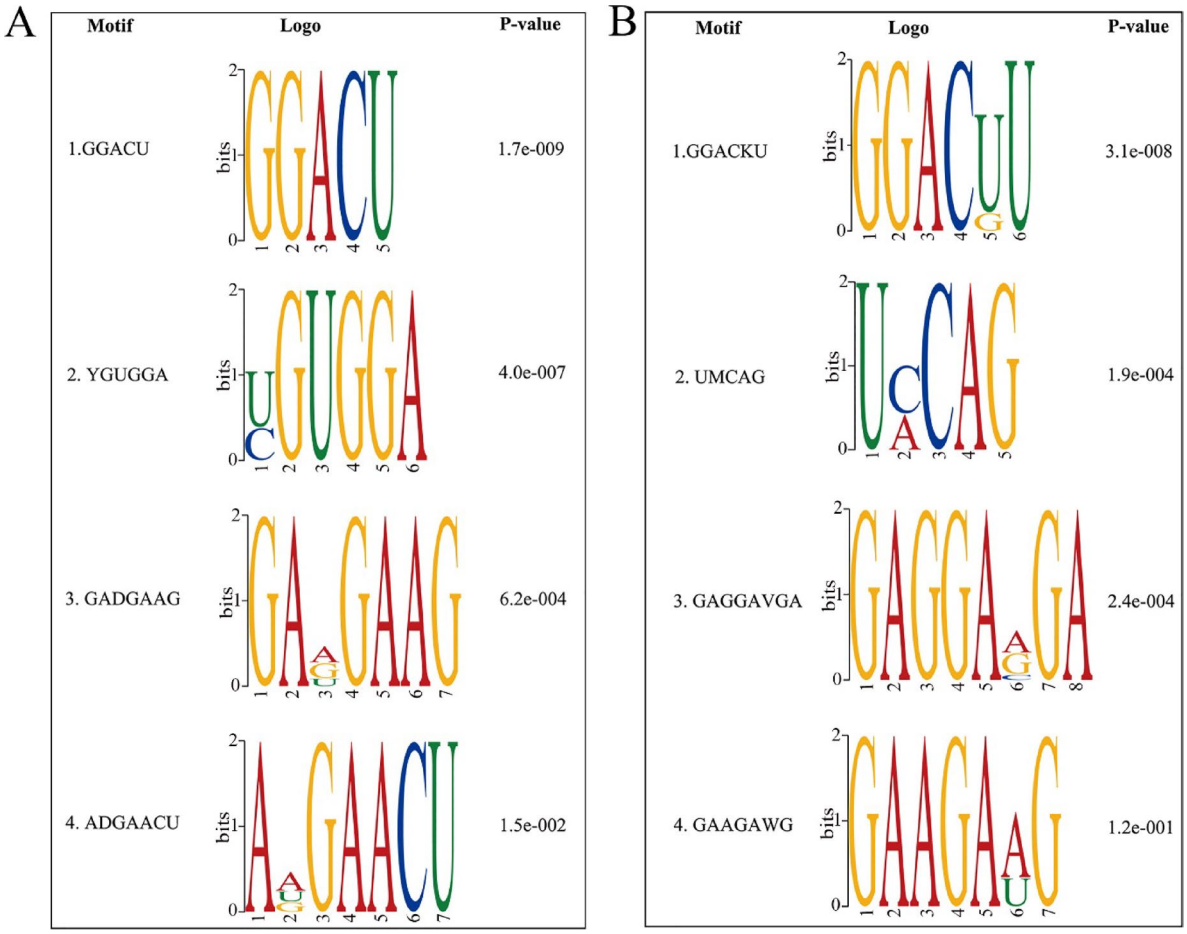

Fig. 3. The motifs enriched in m^{6}A peaks in (**A**) AAA and (**B**) control group.

The *CACNALE, CLASP1, D130043K22RIK, EPHA5, EXOC5, MYT1, PLD5, PXDN, RPUSD2, RREB1 and TRDN* mRNAs contained both hypermethylated and hypomethylated m^{6}A sites, albeit at different locations. The top 10 hyper- and hypomethylated m^{6}A peaks in AAA group are shown in Table 1.

The differentially methylated mRNAs have distinct functional profiles

The putative functions of m^{6}A modification in AAA pathogenesis were further explored by an analysis of the differentially methylated mRNAs using GO and KEGG. As shown in Fig. 4, the top 3 enriched GO terms were transcription coregulator activity (MF category), nuclear body (CC category) and cell surface receptor signaling pathway involved in cell–cell signaling (BP category). More than 40 functional clusters of mRNAs were identified. For the MF category, the mRNAs were grouped into the transcription activity-associated cluster containing transcription coregulator activity, transcription coactivator activity, transcription corepressor activity and DNA-binding transcription repressor activity, and the nucleoside-triphosphatase regulator activity-associated cluster which contained GTPase activator activity, GTPase regulator activity, enzyme activator activity, positive regulation of hydrolase activity and regulation of GTPase activity. For the CC category, mRNAs were involved in nuclear-associated and endosome-associated clusters. Maximum clusters were detected in the BP category, such as cell–cell signaling pathway-associated cluster, which included cell surface receptor signaling pathway, cell–cell signaling by Wnt, Wnt signaling pathway, negative regulation of Wnt signaling pathway, canonical Wnt signaling pathway, regulation of Wnt signaling pathway, negative regulation of canonical Wnt signaling pathway and regulation of canonical Wnt signaling pathway. The top 20 clusters with their representative enriched terms and their network are shown in Fig. 5A,B.

All top 10 GO terms for the hypomethylated mRNAs were in the MF category, including G protein-coupled receptor activity, ion channel activity and substrate-specific channel activity. The most significantly enriched item in the BP category was the response to pheromone. For the CC category, transporter complex showed the highest enrichment score. The top 10 enriched items for each category are shown in Fig. 4. The membership category analysis showed that the hypomethylated mRNAs were classified into less than 20 clusters. The ion channel activity cluster contained 24 members, including substrate-specific channel activity, passive transmembrane transporter activity, voltage-gated potassium channel activity, potassium ion transmembrane transporter activity etc. All enriched clusters are shown in Fig. 5C,D. According to the KEGG pathway analysis, hypermethylated mRNAs were significantly enriched in Wnt signaling pathway, although most genes were involved in pathways

Regulation	Gene name	Location of peak	Fold change	P-value	FDR
Up	COL10A1	chr10: 34394187–34394800	245.48	2.56E-10	3.03E-08
Up	SERPINA1A	chr12:103857424–103857740	86.86	5.86E-08	2.35E-06
Up	BTK	chrX: 134542335–134542540	65.70	2.71E-06	6.50E-05
Up	APOA5	chr9: 46269767–46270700	57.75	6.01E-08	2.41E-06
Up	APOB	chr12:8012141–8012540	56.25	1.34E-09	1.15E-07
Up	MYH6	chr14: 54946312–54946516	47.45	8.09E-12	2.13E-09
Up	GM10273	chr10: 59396181–59396757	38.76	2.05E-11	4.20E-09
Up	FBN2	chr18: 58009821–58010632	33.04	2.17E-09	1.69E-07
Up	APOB	chr12: 8006201–8007020	29.63	4.90E-08	2.03E-06
Up	CD22	chr7: 30877438–30877917	23.49	9.39E-10	8.64E-08
Down	OLFR692	chr7: 105368721–105369355	132.4	1.64E-10	2.13E-08
Down	WFDC6A	chr2: 164579518–164579845	122.4	1.21E-11	2.84E-09
Down	PAX7	chr4: 139737501–139738120	99.4	6.81E-10	6.65E-08
Down	SYCE3	chr15: 89390165–89390439	92.7	3.74E-09	2.60E-07
Down	GSDMC4	chr15: 63891381–63891960	89.7	4.39E-08	1.85E-06
Down	EIF4E1B	chr13:54784004–54784562	86.3	2.28E-07	7.59E-06
Down	FBXW21	chr9: 109145459–109145670	86.3	2.3E-07	7.65E-06
Down	PGLYRP3	chr3: 92,022,604–92,022,806	86.1	1.08E-08	5.98E-07
Down	ZFP719	chr7: 43,591,961–43,592,180	76.3	1.13E-07	4.13E-06
Down	ARHGEF38	chr3: 133,132,040–133,132,282	73.4	8.72E-07	2.42E-05

Table 1. The top 10 differentially methylated m^{6}A peaks in the aorta walls of AAA mice.

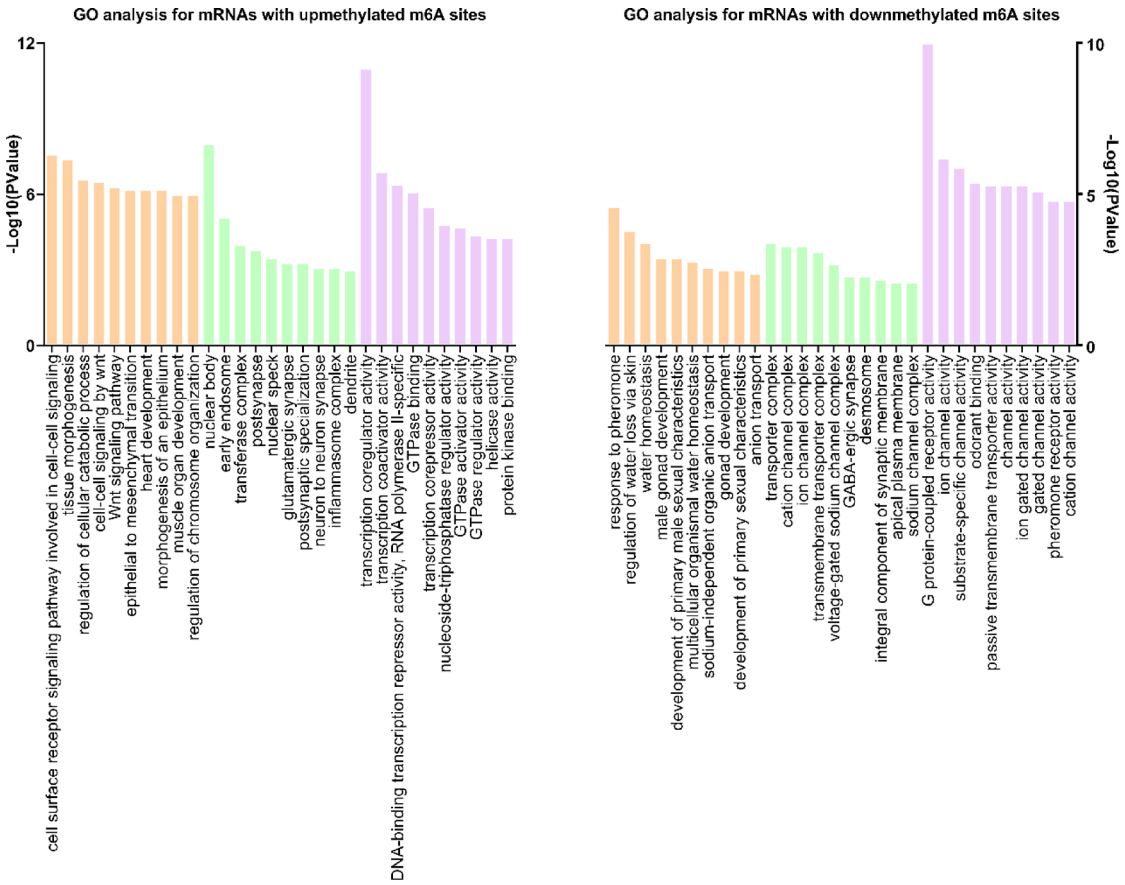

Fig. 4. GO analysis of differentially methylated mRNAs. The top 10 enriched items for each category are shown. The orange represents the biological processes.

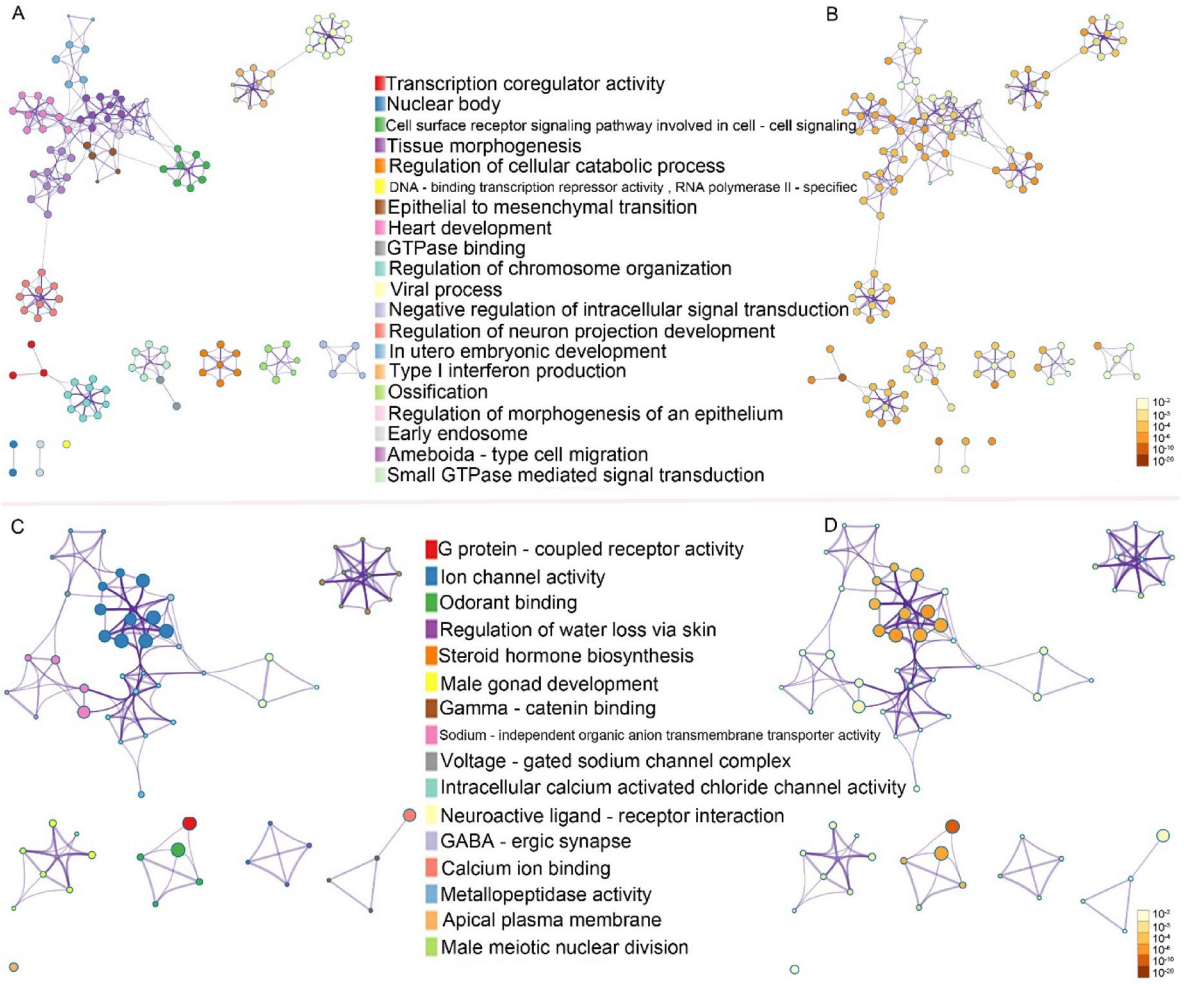

Fig. 5. The network of enriched GO item clusters for the differentially methylated mRNAs. (**A**, **B**) The network of the top 20 clusters for hypermethylated mRNAs. (**A**) Each node represents an enriched item and is color-coded by its cluster ID. The nodes that share the same cluster ID are typically close to each other. (**B**) Each node represents an enriched item and is color-coded by p-value. The items with more genes have a more significant p-value. (**C**, **D**) The network of the total clusters for hypomethylated mRNAs. (**C**) Each node represents an enriched item and is color-coded by its cluster ID. The nodes that share the same cluster ID are typically close to each other. (**D**) Each node represents an enriched item and is color-coded by p-value. The items with more genes have a more significant p-value.

in cancer. For the hypomethylated mRNAs, olfactory transduction pathway had the highest enrichment score and the most counts of differentially methylated genes (Fig. 6).

Verification of methylation of mRNAs and presentation of expression profile of m^{6}A regulators

The results predicted by SRAMP online tool showed that there was one high confidence methylation site in LEF1(located in Chr3: 131,223,134; sequence:AG**A**CU; prediction score:0.635), and four high confidence sites in AXIN1(located in Chr17: 26,143,008; sequence:GG**A**CU; prediction score:0.752. Chr17: 26,143,045; sequence: GG**A**CU; prediction score:0.675. Chr17:26,143,207; sequence:GG**A**CU; prediction score:0.676. Chr17: 26,143,335; sequence:GG**A**CA; prediction score:0.683). The results of MeRIP-qPCR showed that m^{6}A level of LEF1 mRNA and AXIN1 mRNA (region containing Chr17:26,143,207) was significantly higher in AAA group than control group (4.28 ± 1.24 vs. 2.13 ± 0.76, $P = 0.011$; 3.82 ± 1.16 vs. 1.86 ± 0.25, $P = 0.018$, respectively). There was no statistical difference between AAA group than control group in levels of m^{6}A of AXIN1 mRNA (region containing Chr17:26,143,008, Chr17: 26,143,045 and Chr17: 26,143,335) (Fig. 7A). After verifying the accuracy of sequencing, we compared the FPKM values of 23 identified m^{6}A regulators (ALKBH5, FTO, HAKAI, HNRNPA2B1, HNRNPC, IGF2BP1, IGF2BP2, IGF2BP3, KIAA1429, METTL14, METTL16, METTL3, RBM15, RBM15B, VIRMA, WTAP, YTHDC1, YTHDC2, YTHDF1, YTHDF2, YTHDF3, ZC3H13, ZCCHC4)[26] to explore the underlying regulatory mechanism. The *VIRMA* gene was not found. The mRNA expression of *IGF2BP1* gene was 0 in both groups. There were no differentially expressed in the other genes between AAA and control group (Fig. 7B). Then we compared the methylation levels of these 23 genes in the two groups through

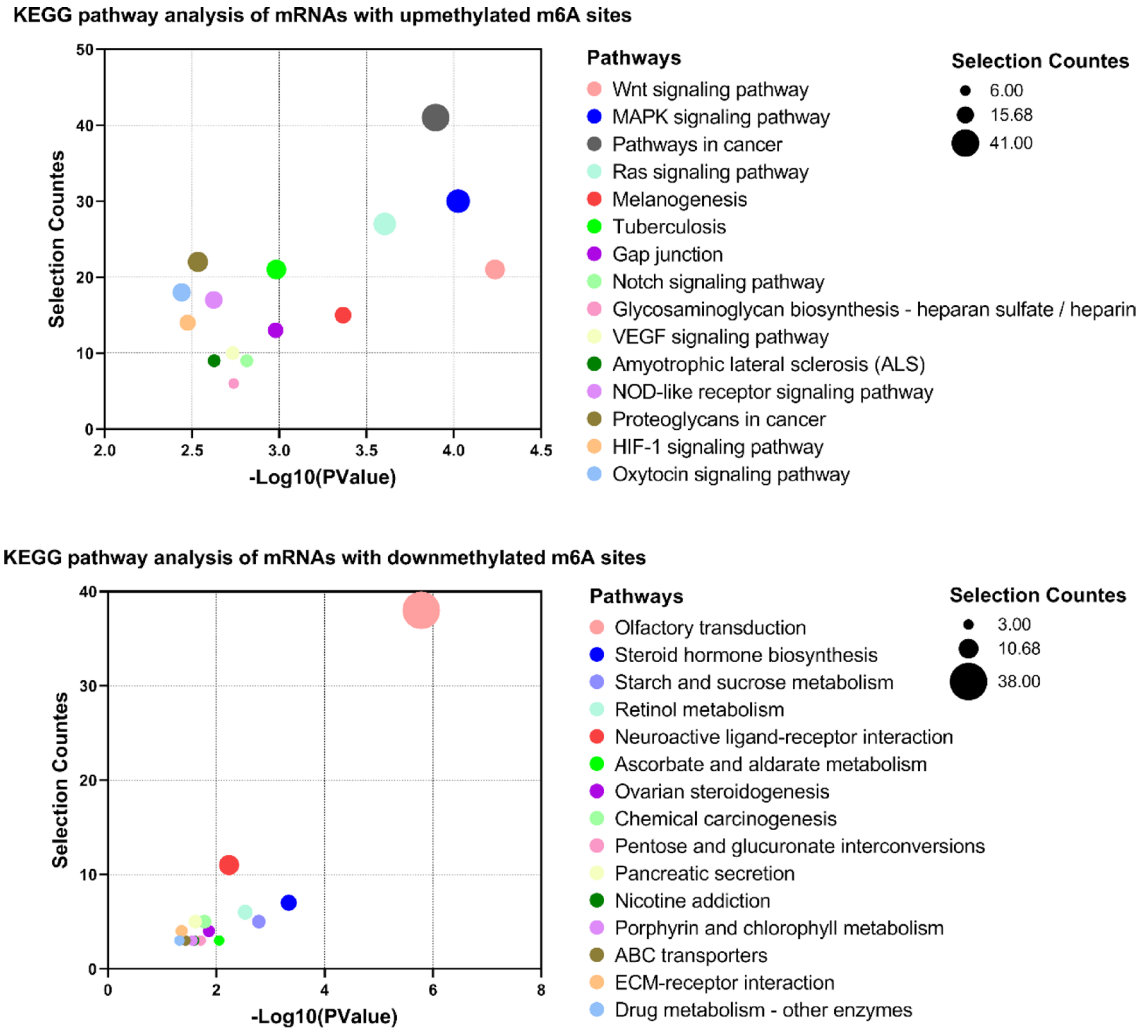

Fig. 6. KEGG analysis of differentially methylated mRNAs. Each bubble represents an enriched pathway and the size indicates the gene count of the pathway.

meRIP-sequencing data. The results showed that the methylation levels of KIAA1429, WTAP, YTHDC1 and ZC3H13 in AAA group increased more than 2 folds when compared to the control group, the fold value of which were 2.77, 2.71, 2.27 and 2.57 with the $P < 0.01$, respectively.

Integrated analysis of m^{6}A-MeRIP sequencing and mRNA sequencing

Integrated analysis of the differentially methylated and differentially expressed mRNA sequencing data showed that 154 mRNAs with 172 hypermethylated m^{6}A sites were upregulated in the AAA group (Supplemental material, S1). In addition, the Kcnd3 and Hspa1a mRNAs with hypomethylated m^{6}A sites were downregulated, and the hypomethylated SEZ6L, D130043K22RIK, SH3GL2, DOCK3, OPCML, EPHA5, CYP4F14 and ATP8B4 mRNAs were upregulated in the AAA group compared to the control group. The top 10 differentially expressed mRNAs with hyper- and hypomethylated m^{6}A sites are shown in Table 2.

Discussion

The m^{6}A methylated modification is a reversible process mediated by methyltransferase complex, demethylases and m^{6}A-binding proteins. While the first two processes occur in the nucleus, both nuclear and cytoplasmic proteins bind to the m^{6}A sites. The m^{6}A modification affects mRNA stability, translation, splicing, location and expression, and therefore modulates multiple physiological and pathophysiological processes, such as neural development, adult brain function, normal and malignant hematopoiesis etc.[27,28]. He et al. were the first to associate abundant m^{6}A modification with poor outcomes of AAA, and identified m^{6}A modulators involved in its pathogenesis. However, the m^{6}A status of the aorta transcriptome in AAA patients has not been profiled so far due to a lack of tissue samples. In this study, we established an Ang II-induced model of AAA in mice to compare the m^{6}A modification levels between normal and diseased aorta.

The AAA group showed more than twofold increase in the m^{6}A peaks and methylated mRNAs compared to the control group. The overall enrichment in m^{6}A modification in the AAA group is consistent with the findings

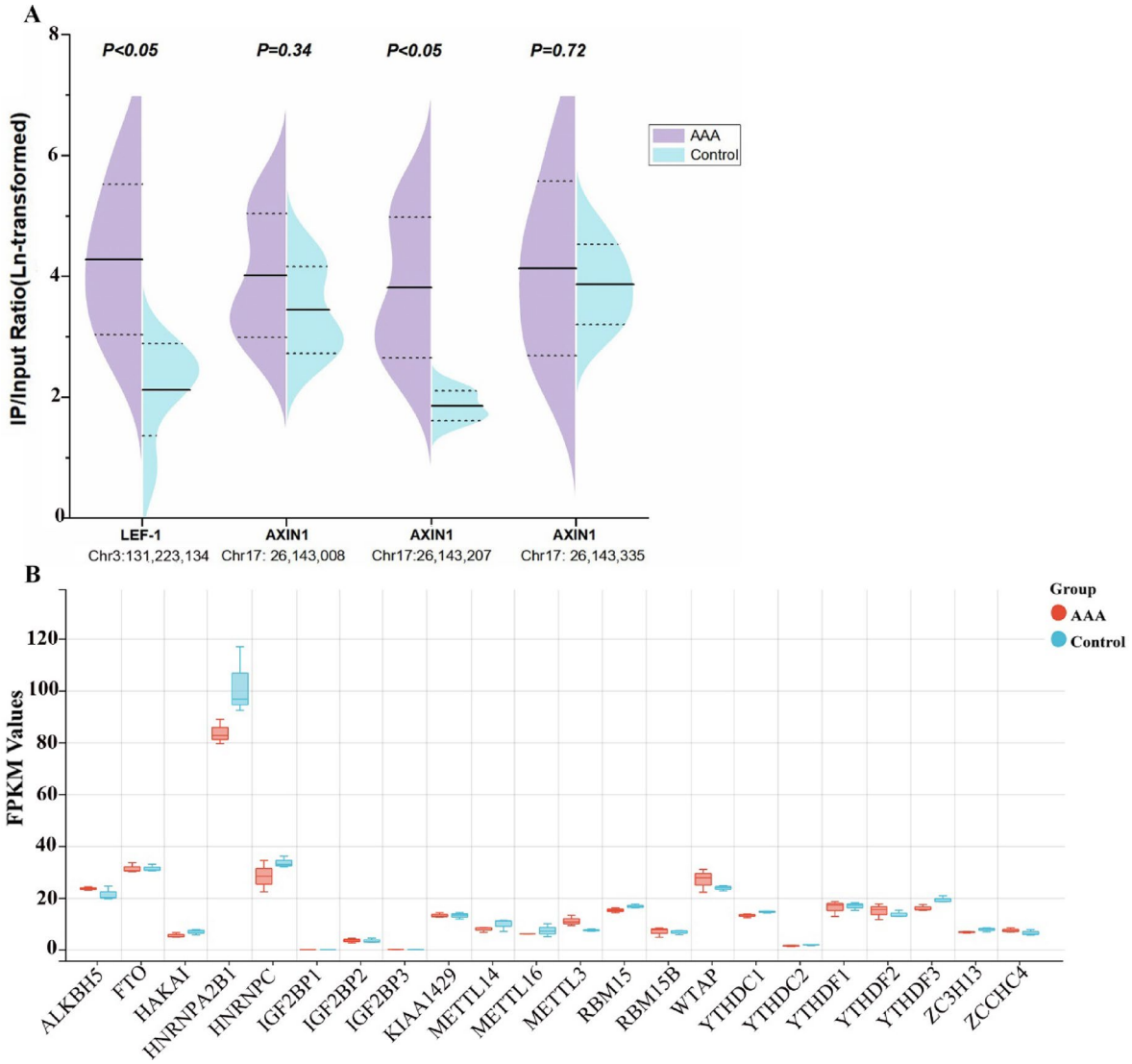

Fig. 7. m^{6}A methylation levels of two genes and mRNA expression profile of m^{6}A regulators. (**A**) The methylation ratio of LEF1 and AXIN1 mRNA in predicted sites in AAA group (n = 5) and control group (n = 5) using MeRIP-qPCR method. (**B**) The FPKM values of 22 identified m^{6}A regulators in AAA group (n = 5) and control group (n = 5). Data derived from mRNA sequencing.

of He et al. in human tissues[12]. Most m^{6}A peaks were located in the CDS and stop codon regions in both AAA and control groups, although the proportion of m^{6}A modification in stop codon region was nearly 5% higher in the former, which is likely associated with enhanced translation of the corresponding transcripts. The integrated analysis of m^{6}A-MeRIP sequencing and mRNA sequencing data showed that mRNAs with hypermethylated m^{6}A sites were usually upregulated, which can be attributed to ribosome reloading and the recruitment of eukaryotic translation initiation factor (eIF3) to the stop codon region[29].

There were 1865 differentially methylated mRNAs in the AAA group, and the majority contained only a single m^{6}A peak as shown in previous reports[30,31]. Interestingly, six hypermethylated m^{6}A sites were observed in the *TTN* transcript in AAA group, which corresponded to higher mRNA levels as well. The *TTN* gene encodes for titin, the largest protein known in humans, and a key component of skeletal and cardiac muscles. It is frequently mutated in striated muscle disorders such as dilated cardiomyopathy and tibial muscular dystrophy[32,33]. However, little is known regarding any potential association between the *TTN* gene and AAA. Based on our findings, we hypothesize that the extent of m^{6}A modification in *TTT* mRNA is a pathological factor in AAA. Mechanistically, m^{6}A possibly regulates phosphorylation and alternative splicing of *TTN* mRNA and enhances its translation of *TTN* gene. In fact, post-transcriptional changes in *TTT* mRNA in vascular smooth muscle cells affect the interaction of titin and actin-myosin II filament-based contractile structures, and mediates atherosclerotic progression[34,35].

Functional annotation showed that the hypermethylated mRNAs in the AAA group were primarily enriched in transcription regulation and intercellular signaling, indicating that the m^{6}A modification mediates AAA development by affecting these functions. In addition, more than 50 hypermethylated mRNAs identified in

Gene	FPKM_AAA	FPKM_control	Log2(FC)	Regulation	m^{6}A location	Log2(FC)	Regulation
MYH6	52.9359	0.106102	8.96	up	chr14:54946312–54946516	5.57	up
APOB	10.8522	0.0749424	7.18	up	chr12:8006201–8007020	4.89	up
APOB	10.8522	0.0749424	7.18	up	chr12: 8006201–8007020	5.81	up
FBN2	1.40266	0.0349152	5.33	up	chr18:58009821–58010632	5.05	up
AZGP1	7.29438	0.305655	4.58	up	chr5:137989561–137990160	3.17	up
NECAB1	1.00697	0.0480568	4.39	up	chr4:14953321–14954120	2.49	up
PHYHIPL	2.07091	0.15345	3.75	up	chr10:70559441–70559740	4.21	up
TTN	22.2403	1.86122	3.58	up	chr2:76729361–76730360	3.59	up
TN	22.2403	1.86122	3.58	up	chr2: 76729361–76730360	3.51	up
TTN	22.2403	1.86122	3.58	up	chr2: 76729361–76730360	3.95	up
TTN	22.2403	1.86122	3.58	up	chr2: 76729361–76730360	3.66	up
TTN	22.2403	1.86122	3.58	up	chr2: 76729361–76730360	3.39	up
TTN	22.2403	1.86122	3.58	up	chr2: 76729361–76730360	3.82	up
ASIC2	2.90899	0.248557	3.55	up	chr11:80880501–80881158	3.6	up
BCL11B	1.44356	0.129653	3.48	up	chr12:107914901–07917240	4.29	up
OBSCN	4.72503	0.446828	3.4	up	chr11: 59038541–9039198	3.96	up
Sh3gl2	2.09791	0.164149	3.68	up	chr4:85388741–85389380	1.42	down
Epha5	3.92818	0.562076	2.81	up	chr5: 84084705–84084915	2.57	down
Sez6l	1.41548	0.218423	2.7	up	chr5: 112419150–12419380	1.73	down
Dock3	4.46441	0.887865	2.33	up	chr9: 107055361–07055604	1.78	down
Atp8b4	2.74836	0.749526	1.87	up	chr2:126337376–26337622	1.92	down
D130043K22Rik	1.26228	0.362255	1.8	up	chr13: 24872218–24872447	1.72	down
Cyp4f14	1.11104	0.390139	1.51	up	chr17: 32909121–32909340	2.53	down
Opcml	1.99407	0.990129	1.01	up	chr9: 28813841–28815460	2.13	down
Kcnd3	4.31286	9.43156	1.13	down	chr3:105667301–105667589	2.59	down
Hspa1a	3.32072	53.6239	4.01	down	chr17: 34971921–34972156	2.29	down

Table 2. The top 10 differentially expressed mRNAs with corresponding hyper- and hypomethylated m^{6}A between AAA group with control group.

this study are involved in Wnt signaling-associated processes. For example, Wnt 11 (wingless-type MMTV integration site family member 11) was enriched in 38 biological processes, including tissue morphogenesis, epithelial to mesenchymal transition, regulation of chromosome organization etc., and involved in 9 out of 10 top ten BP items. We chose two key genes (LEF1 and AXIN1) for validation. LEF1 was a member of transcription factor LEF1/TCF, which served an important role in regulation of canonical Wnt pathway. The hypermethylated site of *LEF1* was located in 3'UTR region, in which the stability, location, or binding ability with β-catenin of LEF1 mRNA might be affected and resulted in the transcriptional dysregulation of Wnt target genes[36]. AXIN1 was also essential in Wnt signaling pathway as its abundance could control the degradation of β-catenin. The hypermethylated site of *AXIN1* was located in CDS region. The methylation modification in CDS region might slow the translation elongation and affect the abundance of AXIN1[37]. The Wnt signaling pathway regulates the formation of coronary vessels, as well as the proliferation, migration and survival of vascular smooth muscle cells, and is frequently dysregulated in cardiovascular diseases including AAA. We detected a significant correlation between m^{6}A modification and Wnt signaling pathway in AAA, which is consistent with previous reports[38,39]. The KEGG pathway analysis further showed that the amyotrophic lateral sclerosis (ALS) pathway had the highest enrichment score. ALS is a neurodegenerative disease that results in motor neuron loss, which leads to muscle weakness and eventually death. This points to a possible neurological basis of AAA which is worth investigating further.

The hypomethylated mRNAs were mainly enriched in G protein-coupled receptor activity, ion channel activity and odorant binding. The ion channel activity cluster included CACNA1E, KCNA4, KCNJ6 and KCNS2 genes. Ion channels play important roles in the contractile activity of vascular smooth muscle cells and regulate the vascular tone[40,41]. Thus, hypomethylation of the ion channel-related mRNAs may disrupt the function of Ca^+ and K^+ channels in vascular smooth muscle and affect normal vascular function, eventually leading to AAA.

Further, to initially explore the mechanism of m^{6}A modification in mice model, we viewed the sequencing data of the methylation levels and mRNA expression of 22 identified common m^{6}A regulators. In the previous studies, m^{6}A-related diseases were often accompanied by changes in the mRNA of one or more regulators[42]. m^{6}A modification was commonly catalyzed by METTL3/ METTL14/ WTAP/ VIRMA/ KIAA1429/ HAKAI/ ZC3H13 complex. Only METTL3 and METTL14 exhibited the methyltransferase activity. KIAA1429, WTAP and ZC3H13 acted by forming a binding site that maximized the catalytic activity of METTL3 and METTL14[43]. But no change in their mRNA expression was observed in our study. Interestingly, the raised m^{6}A modification was observed in the three core members of methyltransferase complex in AAA group, which was rarely been studies.

In conclusion, the aorta walls of AAA model mice showed significant different m^{6}A expression profiles from the control group, which strongly suggested that m^{6}A might be involved in the pathogenesis of AAA, especially the Wnt pathway and G protein receptor related genes worthy of further investigation.

Data availability

Sequence data that support the findings of this study have been deposited in the Gene-Expression Omnibus (GEO; https://www.ncbi.nlm.nih.gov/geo/) with the primary accession code GSE171371.

Received: 26 September 2024; Accepted: 22 May 2025
Published online: 29 May 2025

References

1. Miao, T. et al. Activated invariant natural killer T cells infiltrate aortic tissue as key participants in abdominal aortic aneurysm pathology. *Immunology* **164**, 792–802 (2021).
2. Dahl, M. et al. A population-based screening study for cardiovascular diseases and diabetes in Danish postmenopausal women: Acceptability and prevalence. *BMC Cardiovasc. Disord.* **18**, 20 (2018).
3. Murali Krishna, S., Morton, S. K., Li, J. & Golledge, J. Risk factors and mouse models of abdominal aortic aneurysm rupture. *Int. J. Mol. Sci.* **21**, 7250 (2020).
4. Jonkhout, N. et al. The RNA modification landscape in human disease. *RNA* **23**, 1754–1769 (2017).
5. Wei, W., Ji, X., Guo, X. & Ji, S. Regulatory role of N(6) -methyladenosine (m(6) A) methylation in RNA processing and human diseases. *J. Cell Biochem.* **118**, 2534–2543 (2017).
6. Roundtree, I. A., Evans, M. E., Pan, T. & He, C. Dynamic RNA modifications in gene expression regulation. *Cell* **169**, 1187–1200 (2017).
7. Xiang, J. F. et al. N(6)-methyladenosines modulate A-to-I RNA editing. *Mol. Cell* **69**(126–35), e6 (2018).
8. Li, Y. et al. Molecular characterization, biological function, tumor microenvironment association and clinical significance of m6A regulators in lung adenocarcinoma. *Brief Bioinform.* **22**, 225 (2020).
9. Xu, S., Tang, L., Dai, G., Luo, C. & Liu, Z. Expression of m6A regulators correlated with immune microenvironment predicts therapeutic efficacy and prognosis in gliomas. *Front Cell Dev. Biol.* **8**, 594112 (2020).
10. Huang, T. et al. YTHDF2 promotes spermagonial adhesion through modulating MMPs decay via m(6)A/mRNA pathway. *Cell Death Dis.* **11**, 37 (2020).
11. Zhao, T., Li, X., Sun, D. & Zhang, Z. Oxidative stress: One potential factor for arsenite-induced increase of N(6)-methyladenosine in human keratinocytes. *Environ. Toxicol. Pharmacol.* **69**, 95–103 (2019).
12. He, Y. et al. Increased m6A methylation level is associated with the progression of human abdominal aortic aneurysm. *Ann. Transl. Med.* **7**, 797 (2019).
13. Zhong, L. et al. METTL3 induces AAA development and progression by modulating N6-methyladenosine-dependent primary miR34a processing. *Mol. Ther. Nucleic Acids* **21**, 394–411 (2020).
14. Daugherty, A., Manning, M. W. & Cassis, L. A. Angiotensin II promotes atherosclerotic lesions and aneurysms in apolipoprotein E-deficient mice. *J. Clin. Invest.* **105**, 1605–1612 (2000).
15. Kechin, A., Boyarskikh, U., Kel, A. & Filipenko, M. cutPrimers: A new tool for accurate cutting of primers from reads of targeted next generation sequencing. *J. Comput. Biol.* **24**, 1138–1143 (2017).
16. Kim, D., Langmead, B. & Salzberg, S. L. HISAT: A fast spliced aligner with low memory requirements. *Nat. Methods* **12**, 357–360 (2015).
17. Quinlan, A. R. & Hall, I. M. BEDTools: A flexible suite of utilities for comparing genomic features. *Bioinformatics* **26**, 841–842 (2010).
18. Bailey, T. L. DREME: Motif discovery in transcription factor ChIP-seq data. *Bioinformatics* **27**, 1653–1659 (2011).
19. Olarerin-George, A. O. & Jaffrey, S. R. MetaPlotR: A Perl/R pipeline for plotting metagenes of nucleotide modifications and other transcriptomic sites. *Bioinformatics* **33**, 1563–1564 (2017).
20. Luo, G. Z. et al. Unique features of the m6A methylome in Arabidopsis thaliana. *Nat. Commun.* **5**, 5630 (2014).
21. Shen, L. et al. diffReps: Detecting differential chromatin modification sites from ChIP-seq data with biological replicates. *PLoS ONE* **8**, e65598 (2013).
22. Zhou, Y. et al. Metascape provides a biologist-oriented resource for the analysis of systems-level datasets. *Nat. Commun.* **10**, 1523 (2019).
23. Kanehisa, M. & Goto, S. KEGG: Kyoto encyclopedia of genes and genomes. *Nucleic Acids Res.* **28**(1), 27–30 (2000).
24. Kanehisa, M. Toward understanding the origin and evolution of cellular organisms. *Protein Sci.* **28**(11), 1947–1951 (2019).
25. Kanehisa, M., Furumichi, M., Sato, Y., Kawashima, M. & Ishiguro-Watanabe, M. KEGG for taxonomy-based analysis of pathways and genomes. *Nucleic Acids Res.* **51**(D1), D587–D592 (2023).
26. Zhao, H. et al. m6A regulators is differently expressed and correlated with immune response of esophageal cancer. *Front Cell Dev. Biol.* **9**, 650023 (2021).
27. Livneh, I., Moshitch-Moshkovitz, S., Amariglio, N., Rechavi, G. & Dominissini, D. The m(6)A epitranscriptome: Transcriptome plasticity in brain development and function. *Nat. Rev. Neurosci.* **21**, 36–51 (2020).
28. Vu, L. P., Cheng, Y. & Kharas, M. G. The biology of m(6)A RNA methylation in normal and malignant hematopoiesis. *Cancer Discov.* **9**, 25–33 (2019).
29. Zaccara, S., Ries, R. J. & Jaffrey, S. R. Reading, writing and erasing mRNA methylation. *Nat. Rev. Mol. Cell Biol.* **20**, 608–624 (2019).
30. Linder, B. et al. Single-nucleotide-resolution mapping of m6A and m6Am throughout the transcriptome. *Nat. Methods* **12**, 767–772 (2015).
31. Meyer, K. D. et al. Comprehensive analysis of mRNA methylation reveals enrichment in 3' UTRs and near stop codons. *Cell* **149**, 1635–1646 (2012).
32. Pollazzon, M. et al. The first Italian family with tibial muscular dystrophy caused by a novel titin mutation. *J. Neurol.* **257**, 575–579 (2010).
33. Tharp, C. A., Haywood, M. E., Sbaizero, O., Taylor, M. R. G. & Mestroni, L. The giant protein titin's role in cardiomyopathy: genetic, transcriptional, and post-translational modifications of TTN and their contribution to cardiac disease. *Front. Physiol.* **10**, 1436 (2019).
34. Chi, R. J., Simon, A. R., Bienkiewicz, E. A., Felix, A. & Keller, T. C. 3rd. Smooth muscle titin Zq domain interaction with the smooth muscle alpha-actinin central rod. *J. Biol. Chem.* **283**, 20959–20967 (2008).
35. Keller, T. C., 3rd, Eilertsen, K., Higginbotham, M., Kazmierski, S., Kim, K. T. & Velichkova, M. Role of titin in nonmuscle and smooth muscle cells. *Adv. Exp. Med. Biol.* **481**, 265–77; discussion 78–81 (2000).
36. Santiago, L., Daniels, G., Wang, D., Deng, F. M. & Lee, P. Wnt signaling pathway protein LEF1 in cancer, as a biomarker for prognosis and a target for treatment. *Am. J. Cancer Res.* **7**, 1389–1406 (2017).

37. Mao, Y. et al. m(6)A in mRNA coding regions promotes translation via the RNA helicase-containing YTHDC2. *Nat. Commun.* **10**, 5332 (2019).
38. He, Y. et al. Kallistatin correlates with inflammation in abdominal aortic aneurysm and suppresses its formation in mice. *Cardiovasc. Diagn. Ther.* **10**, 107–123 (2020).
39. Li, J., Krishna, S. M. & Golledge, J. The potential role of Kallistatin in the development of abdominal aortic aneurysm. *Int. J. Mol. Sci.* **17**, 1312 (2016).
40. Dogan, M. F., Yildiz, O., Arslan, S. O. & Ulusoy, K. G. Potassium channels in vascular smooth muscle: A pathophysiological and pharmacological perspective. *Fundam. Clin. Pharmacol.* **33**, 504–523 (2019).
41. Nieves-Cintron, M., Flores-Tamez, V. A., Le, T., Baudel, M. M. & Navedo, M. F. Cellular and molecular effects of hyperglycemia on ion channels in vascular smooth muscle. *Cell Mol. Life Sci.* **78**, 31–61 (2021).
42. Huang, J., Zhou, W., Hao, C., He, Q. & Tu, X. The feedback loop of METTL14 and USP38 regulates cell migration, invasion and EMT as well as metastasis in bladder cancer. *PLoS Genet* **18**, e1010366 (2022).
43. Uddin, M. B., Wang, Z. & Yang, C. The m(6)A RNA methylation regulates oncogenic signaling pathways driving cell malignant transformation and carcinogenesis. *Mol. Cancer* **20**, 61 (2021).

Author contributions

All authors participated in the design, interpretation of the studies and analysis of the data and review of the manuscript; JLW, TYM and YYW have made substantial contributions to conception and design and drafting the manuscript; JLW and ZH contribution to construction of mice model; TYM, WYY, THW, FX, DY, QG,YY and ZCT were involved in analysis of data; BH and JCZ agreed to be accountable for all aspects of the work in ensuring that questions related to the accuracy or integrity of any part of the work are appropriately investigated and resolved.

Funding

This research was funded by National Natural Science Foundation of China (No. 82200528).

Declarations

Institutional Review Board Statement

The animal study protocol was approved by The Animal Care and Use Ethics Committee of West China Second University Hospital, Sichuan University (No.2018084).

Competing interests

The authors declare no competing interests.

Additional information

Supplementary Information The online version contains supplementary material available at https://doi.org/10.1038/s41598-025-03760-8.

Correspondence and requests for materials should be addressed to B.H. or J.Z.